Tunable IR perfect absorbers enabled by tungsten doped VO₂ thin films ⊘

Maria Cristina Larciprete ✉ ⓘ ; Daniele Ceneda ⓘ ; Daniele Scirè ⓘ ; Mauro Mosca ⓘ ;
Dominique Persano Adorno ⓘ ; Sina Abedini Dereshgi ⓘ ; Roberto Macaluso ⓘ ; Roberto Li Voti ⓘ ;
Concita Sibilia ⓘ ; Tiziana Cesca ⓘ ; Giovanni Mattei ⓘ ; Koray Aydin ⓘ ; Marco Centini ⓘ

Check for updates

CrossMark

View Online

Export Citation

AIP Publishing

Tunable IR perfect absorbers enabled by tungsten doped VO₂ thin films

View Online   Export Citation   CrossMark

Maria Cristina Larciprete,[1,a] (ID) **Daniele Ceneda**,[1] (ID) **Daniele Scirè**,[2] (ID) **Mauro Mosca**,[2] (ID) **Dominique Persano Adorno**,[3] (ID) **Sina Abedini Dereshgi**,[4] (ID) **Roberto Macaluso**,[2] (ID) **Roberto Li Voti**,[1] (ID) **Concita Sibilia**,[1] (ID) **Tiziana Cesca**,[5] (ID) **Giovanni Mattei**,[5] (ID) **Koray Aydin**,[4] (ID) and **Marco Centini**[1] (ID)

AFFILIATIONS

[1] Dipartimento di Scienze di Base ed Applicate per l'Ingegneria, Sapienza Università di Roma, Rome, Italy
[2] Department of Engineering, University of Palermo, Viale delle Scienze, Ed. 9, Palermo 90128, Italy
[3] Department of Physics and Chemistry "E. Segré," University of Palermo, Viale delle Scienze, ed. 18, Palermo 90128, Italy
[4] Department of Electrical and Computer Engineering, Northwestern University, Evanston, Illinois 60208, USA
[5] Department of Physics and Astronomy, University of Padova, via Marzolo 8, I-35131 Padova, Italy

a) Author to whom correspondence should be addressed: mariacristina.larciprete@uniroma1.it

ABSTRACT

The temperature tunability of complex dielectric constants of vanadium dioxide (VO₂) makes it a promising phase-change material for use in active, dynamic, tunable photonics applications. Specifically, the semiconductor-to-metal phase transition in VO₂ enables reversible, broadband, and large complex refractive index variation and paves the way for a plethora of applications. Although the critical temperature for phase-transition is $68\,^\circ$C for VO₂ films, its transition temperature can be reduced to room temperature by tungsten-doping of vanadium dioxide. Such a degree of freedom in controlling the critical temperature through tungsten doping provides further tunability of the thermochromic behavior. In this work, we investigate a variety of W-doped VO₂ thin films deposited by laser ablation of targets with increasing W doping content and report detailed infrared characterization together with numerical simulations. Our experimental results indicate that the perfect absorption can be achieved at different temperatures, within the VO₂ insulator-to-metal phase transition process, as a function of W doping content. Tunable subwavelength layers allow perfect absorption under different temperature conditions around $\lambda = 12\ \mu$m. We show that a high dynamic range of reflectivity can be achieved when the temperature is increased above the phase transition temperature. Furthermore, we observe perfect absorption at 11.8 μm at room temperature for a W content of 0.75%. We believe that W-doped VO₂ thin films with tunable and controllable perfect absorption will open the way for a class of promising thermo-optical devices including thermos-photovoltaics, infrared filters, radiative cooling devices, and thermal emitters.

INTRODUCTION

The study of perfect light absorption received wide interest in recent years and utilized in several applications including thermal emitters,[1] optical modulators,[2] and biosensors.[3]

Following the introduction of radar devices, the first perfect absorbers were proposed by Salisbury.[4] A so-called Salisbury screen consists of an absorbing layer placed on top of a thick metal plane and separated by a dielectric spacer. Here, the mechanism of perfect absorption is driven by the thickness of the dielectric spacer to achieve destructive interference of the reflected light between the absorbing layer and the reflective metal background.[1]

Advances in nanophotonics have led to an extreme interest in perfect absorbing devices thanks to the exploitation of different mechanisms in the visible range as well as toward the mid infrared (IR) range. In recent years, it has been demonstrated, both theoretically and experimentally, that perfect absorption can be achieved in systems, such as metamaterials,[5] metasurfaces,[6] multilayer,[7] or single layer devices.[8]

Different geometries have been employed such as resonant Fabry–Perot (FP) like-optical cavity configurations to enhance both

absorption and dynamic range at desired resonance wavelengths. A typical example is the asymmetric Fabry–Perot (FP) cavity consisting of a dielectric layer sandwiched between a semi-transparent mirror and a thick metal layer acting as a full back-reflector.[4] This geometrical configuration enables strong coupling between light and matter and has been employed for reflectivity modulators, and resonant-cavity enhanced (RCE) photodetectors.

Plasmonic metasurfaces, whose typical experimental absorption values range between 90% and as high as 99%, are intensively studied to get perfect absorption and have been demonstrated over a wide range of frequencies.[9] The use of nonlinear metasurfaces[3] to switch from complete to partial absorption by tuning the pump beam intensity allowed coherent perfect absorption as well as control of the relative phases of the input beams. With respect to the asymmetric FPs, these nanostructured devices are more compact with their subwavelength thicknesses but require complex nanofabrication steps, making them very challenging for device applications.

More recently, a new class of low-index materials called epsilon-near-zero (ENZ) materials has attracted much attention. Perfect absorption has been achieved using the ENZ materials in the linear regime.[10,11] In ENZ materials, such as indium tin oxide (ITO) and aluminum-doped zinc oxide (AZO), the real part of the permittivity goes to zero at a particular frequency ENZ, thus exhibiting a huge electric field enhancement.

Moreover, tunable perfect absorption has been experimentally and theoretically investigated in systems, such as graphene,[12] liquid crystals,[13] and phase-change materials (PCMs).[4] Tunable devices based on graphene were exploited in Ref. [14] where it is shown gate voltage-dependent tunable absorption.

Although it is generally assumed that dielectric based perfect absorbers cannot be thinner than the operating wavelength and that plasmonic nanostructures are more compact with their sub-wavelength thicknesses, it was demonstrated, by Kats *et al.*, perfect absorption at about the transition temperature from a $\lambda/65$ thick VO_2 single layer thin film.[5] Additionally, spectral responses in such perfect absorbers can be dynamically tuned by applying voltage or current bias.

Phase-change materials undergo a semiconductor to metal phase transition at a specific phase transition temperature. Among the different thermochromic materials such as niobium dioxide (NbO_2) and vanadium sesquioxide (V_2O_3), VO_2 is widely employed due to its lower phase transition temperature, $T_c = 341$ K ($68\,^\circ$C).[15] VO_2 is a very promising tunable polar material used in diverse applications where a high dynamic range is required.[16] The phase transition from an insulating monoclinic phase into a metallic tetragonal (rutile) phase is accompanied by drastic changes in optical, electrical, and magnetic properties. Tunable optical properties of VO_2 due to phase transition have received a burgeoning amount of interest from the scientific community in recent years. In particular, the thermal emissivity variation activated by temperature in VO_2 in the visible,[17] the IR,[4,18,19] and THz ranges[20] has been demonstrated.

In this work, we investigate a tunable perfect absorber composed of a lithography-free, ultra-thin film of vanadium dioxide (VO_2) on a sapphire substrate inspired by an earlier work.[5] It has been shown that an intermediate state of the insulator–metal phase transition (IMT) in VO_2 arises around the transition temperature, displaying multiple co-existing phases, thus resulting in an effective medium with tunable optical properties in the infrared range. Specifically, experimental results demonstrated that the absorption coefficient can be extremely enhanced in proximity to the phase transition temperature resulting in perfect absorption at a given wavelength and temperature. Thermal control of phase coexistence was still required in order to get the minimum reflectivity condition and enable a high dynamic range of the absorption from 20% to 99.75% at $\lambda = 11.6\ \mu$m.[5]

Here, we investigated a set of VO_2 samples prepared using different amounts of W dopants using pulsed laser deposition (PLD) technique. The thermal tuning of the phase co-existence was found to be preserved in the W-doped VO_2 films. Moreover, we found that by increasing W doping concentration, the absorption enhancement observed at the phase transition temperature ($68\,^\circ$C) can be reduced to room temperature. Thus, our investigated thin films enable perfect absorption at room temperature within a subwavelength thickness. Such a simple thin-film architecture could enable advances in different IR application areas, such as modulators, control of thermal radiation, tunable radiative cooling, thermoregulating layers, thermal emitters, and bolometers.

MEASUREMENTS

W-doped VO_2 thin films were grown using pulsed laser deposition (PLD), an adaptable and low-cost deposition technique that had been previously employed for the deposition of high quality VO_2 films[21–23] and other metal oxides, such as MoO_3,[24] ZnO,[25] AZO,[26] TiO_2,[27] and Nb_2O_5.[28] Furthermore, PLD can be properly adapted to obtain W doped VO_2 films using different doping contents ranging from 0.1% to 10%.

The PLD system employed is described in detail elsewhere.[26] A Q-switched Nd: YAG laser (Quantel mod. YG78C20, $\lambda = 355$ nm) with a pulse width of 6 ns and a repetition rate of 4 Hz was employed as the laser source. Pulses energy of 45 mJ allowed to maintain energy density at 2.5 J cm^{-2}. The VO_2 targets were prepared by cold pressing VO_2 powder (Sigma-Aldrich, purity 99.999%) together with WO_3 powder with different weights, which allowed to achieve targets of W-doped VO_2 with at. concentration ranging from 0.1% to 10%. All films were deposited onto sapphire substrates at the same conditions ($550\,^\circ$C and 10^{-2} mbar oxygen pressure).

IR reflectivity measurements were performed using an FT-IR interferometer (Invenio-R, Bruker) in the spectral range of 4–14 μm. We use a glow-bar as the IR source and deuterated triglycine sulfate (DTGS) photo-voltaic element as the IR detector. A total of 64 interferograms were acquired for each measurement, with a spectral resolution of 2 cm^{-1}. Knife edge apertures were set to 3×3 mm^2 to select a defined sample area during IR data acquisition. The FT-IR platform is equipped with a reflectance unit allowing to set the angles of incidence and reflectance, from almost normal incidence (about $13\,^\circ$) to grazing angles ($85\,^\circ$). For each sample, a set of measurements was performed at the incidence angle of $15\,^\circ$ under different temperatures. The polarization state of incident light can be selected using a wide-range holographic polarizing filter with a motorized mounter. Before each measurement run, the reflectance spectra were recorded at both room temperature and at about $100\,^\circ$C so that the phase transition of VO_2 is completed using two different, crossed, linear polarization states of the incoming light. However, the experimental

11, 091107-2

spectra measured at about normal incidence (15°) show that there is no significant difference between the s- and p-polarized light except for the anisotropy of the Sapphire substrate, clearly visible around 12 μm wavelength in Fig. S1 of the supplementary material section. Because of the lack of in-plane anisotropy, these small discrepancies between s- and p-polarized reflectivity are going to disappear at perfectly normal incidence conditions. For each sample, we report FT-IR spectra in reflection mode at a 15° incidence angle using s-polarized light as a function of temperature by using a portable heating stage, which allowed us to increase the temperature up to 100 °C. Different incidence angles and polarizations were also investigated and reported for completeness in the supplementary material file (Figs. S1–S5).

According to Kirchoff's law of energy conservation, total light absorption at a given frequency is achieved when both reflection and transmission vanish. Optical IR reflection spectra of the undoped VO$_2$ films, displayed in Fig. 1, unveil a clear phase transition when the temperature increases to 100 °C along with a remarkable enhanced and reversible tunability of IR reflectivity spectra. Furthermore, a near zero-reflectivity dip was observed around the nominal phase transition temperature of VO$_2$, which is in agreement with the results observed in Ref. 5.

During the phase-transition process, the coexistence of the two phases is witnessed by the changes in the FT-IR spectral features. Around the phase transition temperature, the VO$_2$ can be modeled as an effective medium[29,30] composed of a semiconductor matrix where the metallic phase emerges as a random dispersion of metallic inclusions whose filling factor spans from 0 (pure semiconductor phase at low temperatures) to 1 (pure metallic phase once phase transition is completed). Different homogenization approaches can be used to model the effective dielectric permittivity in systems composed of randomly dispersed metallic inclusions into a dielectric matrix.[31] Both Maxwelll-Garnett (MG)[32] and Bruggeman[33] models have been used in the literature to describe the effective medium
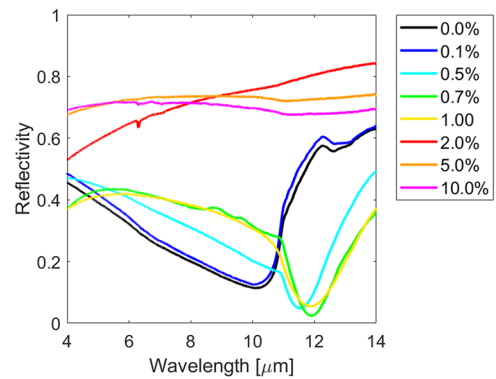

FIG. 2. FT-IR reflectivity spectra measured at room temperature, at a 15° incidence angle from several VO$_2$ films, about 480 nm thick, with increasing W doping at different concentrations, from 0% to 10%.

properties of the VO$_2$ film. Due to the reduced thickness of the investigated VO$_2$ films, metallic inclusions are assumed to have disk-like shapes, as also reported in Refs. 34 and 35.

Here, the Maxwell Garnett (MG) model is adopted, and the effective dielectric permittivity is given by the expression,

$$\varepsilon_{eff,j} = \varepsilon_e + f \frac{\varepsilon_e(\varepsilon_i - \varepsilon_e)}{\varepsilon_e + (1-f)L_j(\varepsilon_i - \varepsilon_e)}, \quad with \; j = x, y, z, \quad (1)$$

where ε_e and ε_i stand for the relative permittivity of the host (semiconducting) matrix and the (metallic) inclusions while the inclusions content ratio in the effective medium is taken into account through the filling factor parameter (f). The shape effects of the dielectric inclusions are taken into account by the depolarization factors, L_j, calculated along the three axes of the ellipsoidal inclusion in the three orthogonal directions, whose values depend on the ratio
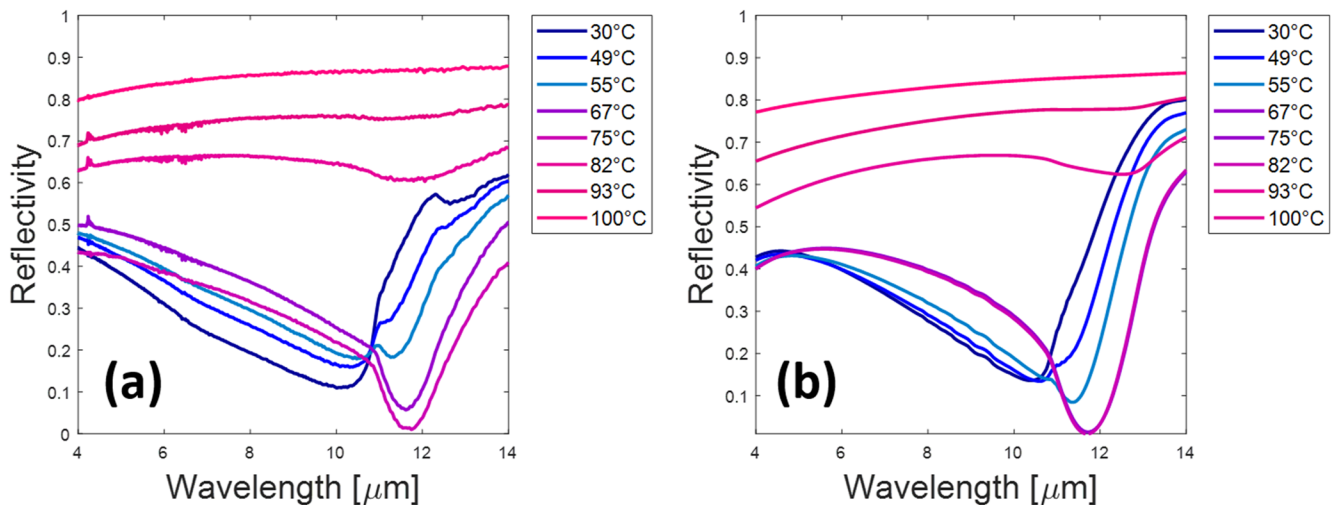

FIG. 1. (a) Reflectivity spectra measured at a 15° incidence angle from a VO$_2$ film, about 480 nm thick grown onto sapphire substrate using pulsed laser deposition. The temperature was varied from 30 to 100 °C. At 75 °C, a drop of the reflectivity value down to 0.02 is observed at λ = 11.8 μm. (b) Calculated reflectivity spectra at temperatures from 30 to 100 °C.

between ellipsoid axes. Specifically, for the discoidal shape of inclusions, the depolarization factors, L_j, are set to 0 along disk diameters (x- and y-directions) while $L_z = 1$. In this case, the MG approach produces the same results as the Looyenga effective medium mixing rules (i.e., a static solution for a planar mixture) successfully adopted in Ref. 36. Following these approaches, the effective dielectric permittivity is calculated starting from the permittivities of the semiconductor and the metal phases.[37] Considering different metallic phase contents, i.e., different filling factors, it is possible to retrieve the corresponding complex refractive index of the investigated film for each temperature. Experimental spectra were, thus, numerically reconstructed for each temperature using a transfer-matrix method (TMM).[38,39] We note that there is an intermediate phase resulting in refractive index matching to the substrate, where the VO_2 layer acts as an antireflection coating, and minimizing the reflected signal with near 0% reflectivity. Zero-reflectivity implies perfect absorption

of the light through the substrate[40] (IR transmission of fused silica substrate at 12 μm wavelength is negligible).

Next, we measured IR reflectivity spectra from different samples of VO_2 films with varying W doping concentrations under similar temperature conditions. W-doping of VO_2 thin films was previously used to decrease the critical temperature. When an increasing content of W doping is included in the VO_2 films, our experiments indicate that although phase transition can still be achieved by changing the temperature, the phase-transition temperature is lowered with increasing W concentration. As a direct consequence, room temperature experimental reflectivity spectra from VO_2 samples with different W concentration displays a different behavior. Specifically, once all the spectra are plotted onto the same graph (see Fig. 2), the different reflectivity spectra resemble somehow the phase transition, in both spectral features and amplitude. However, here, the temperature is fixed to room temperature while the doping
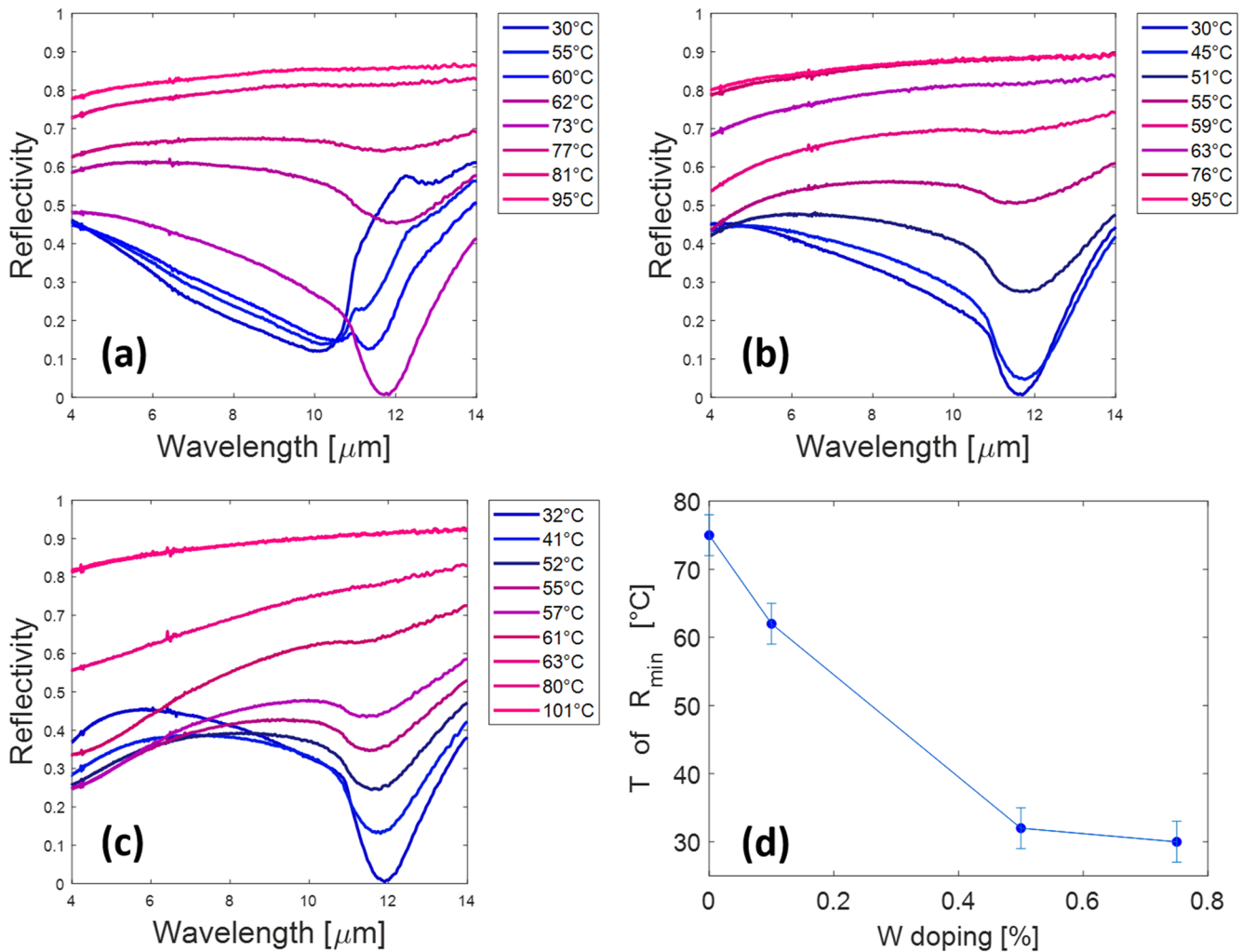

FIG. 3. Temperature-dependent reflectivity spectra measured at a 15° incidence angle from a set of VO_2 films, about 480 nm thick, with increasing W doping concentration: (a) W 0.1%, (b) W 0.5%, and (c) W 0.75%. (d) Temperature corresponding to the minimum of reflectance as a function of W doping.

content is increased and represents the driving force for observed changes.

For a better understanting of how the phase transition is modified when the W is introduced into the VO$_2$ lattice, we measured the reflectivity spectra as a function of temperature for each sample. The semiconductor to metal transition is clearly visible up to an amount of W of about 1%. A further increase of doping content results in films displaying pure metallic behavior, i.e., high reflectivity values at both room temperature and higher temperatures; thus, it is not possible to observe the phase transition. Furthermore, once looking at the spectra taken at different temperatures, we show that zero-reflectivity still appears in each set of measurements [Figs. 3(a)–3(c)]; however, it is shifted forward to lower temperatures as denoted in Fig. 3(d).

The largest dynamic range of reflectivity values, from nearly 2% to about 87%, is still obtained around λ = 11.8 μm, at temperatures of 62, 32, and 30 °C, for 0.1%, 0.5%, and 0.75% tungsten content, respectively. The latter result is particularly exciting since the experimental data obtained from a W doping amount of only 0.75% show that the zero-reflectivity condition, i.e., perfect absorption condition, is accessible at room temperature, i.e., without the need to heat the film.

For completeness, we investigated the reflectivity at different incident angles. As a general feature, the low reflectivity values observed at different temperatures at about λ = 11.8 μm and λ = 11.9 μm, for different W doping content, increase for higher incident angles, leading to a detrimental effect on the perfect absorption behavior and a stronger geometrical anisotropy related to the planar geometry. The experimental spectra obtained at 15°, 30°, and 45° are reported in the supplementary material section (Figs. S1–S5). However, we show in Fig. S5 that for s-polarization, the minimum reflectivity goes from 2% (at 15°) to 12% (at 45°). We note in Fig. 3(c) that for the proper amount of W doping (0.75%), we

can monotonically tune the reflectivity value by increasing the temperature having a one-to-one correspondence between temperature and reflectivity in a wide dynamical range.

When data are displayed as a function of wavelength and temperature, as in Fig. 4, for all investigated samples, a bright band denoted as metallic VO$_2$ (M-VO$_2$) can be highlighted above the transition temperature as the reflectivity value increases due to the metallic behavior of transitioned VO$_2$. As the W% content is increased, the metallic behavior band spreads to lower and lower temperatures. More interestingly, the reflectivity values measured at the wavelength corresponding to perfect absorbing behavior display a wide monotonic dynamic range, which can be achieved by increasing the temperature, starting from room temperature as shown in Fig. 5 (red curve). We note that the experimental data can be fitted with an adapted sigmoidal function with fit parameters a, b, and c, with y being the fitted reflectivity and x being the temperature in °C,

$$y = \frac{a}{\left[e^{(-bx+c)} + 1 \right]}. \tag{2}$$

The obtained fit, with $a = 0.92$, $b = 0.22\,°\text{C}^{-1}$, and $c = 12.50$, gives a $R^2 = 0.98$.

On the other hand, the undoped sample displays a temperature behavior that is not monotonically defined (blue dots). The blue curve in Fig. 5 has been obtained with a MATLAB-generated smoothing spline, and it is intended only as a guide for the eyes.

This result opens interesting perspectives for further development of thermoregulation devices, IR optical limiters, and adaptive camouflage coatings operating at room temperature. Furthermore, the obtained experimental findings in terms of wide range tunable reflectivity vs temperature can be extremely interesting for surface phonon polaritons (SPhP) tuning when the W-doped VO$_2$ layer is combined with a layer of another polar material.[16] For example, it
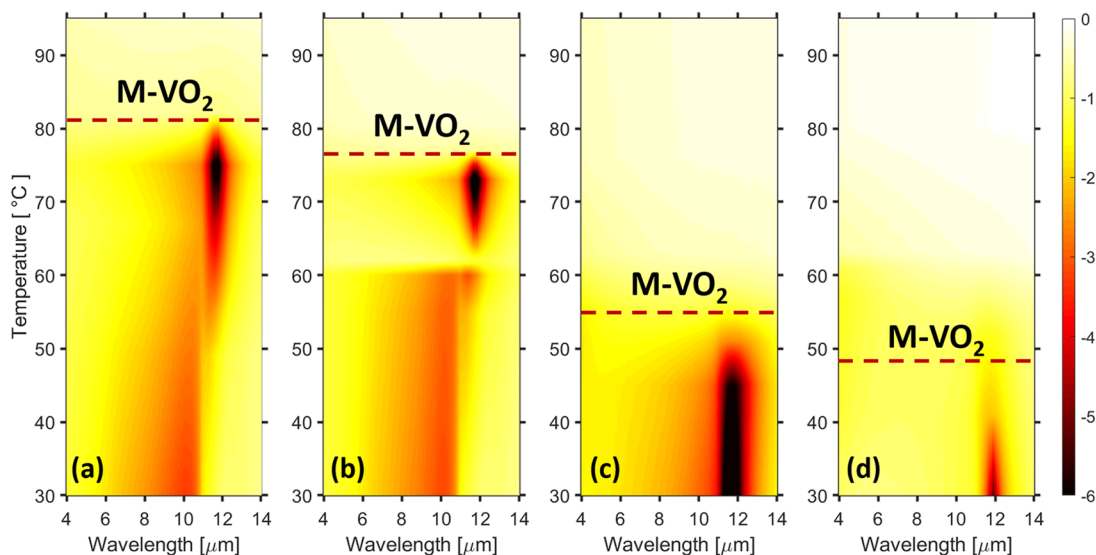
FIG. 4. Reflectivity values plotted, in logarithmic scale, as a function of wavelength and temperature for increasing W doping concentration: (a) W 0.0%, (b) W 0.10%, (c) W 0.50%, and (d) W 0.75%.
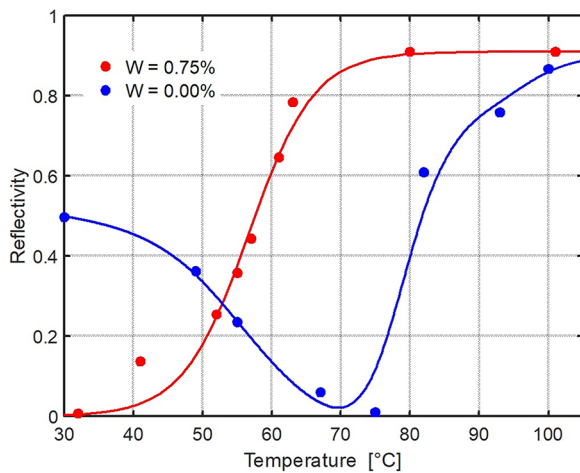
FIG. 5. Reflectivity values plotted as a function of temperature for λ = 11.8 μm (W = 0.00%) and λ = 11.9 μm (W = 0.75%), respectively. The red continuous line is fit with an adapted sigmoidal function (R^2 = 0.98), while the blue line is a MATLAB-generated smoothing spline (R^2 = 0.97) intended as a guide for the eyes.

could be possible to control topological transitions from hyperbolic SPhP to normal SPhP by adding a natural hyperbolic material layer, such as α-MoO₃[41] or β-Ga₂O₃.[42] This could increase the versatility and useable range of sensing devices based on SPhP excitation and overcome the intrinsic mechanical limits of twisted layers tunability.

CONCLUSIONS

In conclusion, we experimentally investigated VO_2 films and prepared them with different contents of W doping using pulsed laser deposition, to control and tune the spectral features over temperature. Due to its phase transition from monoclinic (semiconductor) to tetragonal (metallic) lattice structure at the temperature of 68 °C, accompanied by both physical and optical properties variation, VO_2 offers rich physical phenomena that pave the way to a plethora of dynamic applications. Furthermore, the tensile strain introduced by W doping within the lattice structure supports the stabilization of the metallic phase with respect to the semiconducting phase.[43] We experimentally investigated the film reflectivity in the range of 4–14 μm, and our experimental findings show remarkable features of perfect absorption in the obtained films. A strong modulation of VO_2 film infrared reflectivity with temperature has been experimentally observed. In particular, we show that the infrared optical response of the tunable film can be modulated from complete to partial absorption by changing the applied temperature. The undoped VO_2 displays a reflectivity minimum at λ = 11.8 μm at the conventional transition temperature for this material, i.e., at about 68 °C with a dynamic range as high as ΔR = 85%. Interestingly, when W doping is added to the VO_2 lattice, the phase transition temperature along with the minimum reflectivity value, is shifted down to room temperature, thus the perfect absorber behavior becomes accessible even at room temperature.

Moreover, the obtained wide dynamic range of reflectivity can be achieved by monotonically increasing the temperature, starting from room temperature. This large tunability may have great

potential for applications, such as tunable emitters, infrared camouflage, tunable metamaterials, SPhP-based sensing devices, smart windows, and active radiative cooling.

SUPPLEMENTARY MATERIAL

The supplementary material details measurements obtained using two different, crossed, linear polarization states of the incoming light, i.e., s- and p-polarization, for two of the investigated samples at 15° and 30° angles of incidence (Figs. S1–S4). It also includes (Fig. S5) experimental spectra obtained at 15°, 30°, and 45° for one of the samples (W = 0.75%).

AUTHOR DECLARATIONS

Conflict of Interest

The authors have no conflicts to disclose.

Author Contributions

Maria Cristina Larciprete: Conceptualization (equal); Data curation (equal); Investigation (equal); Methodology (equal); Writing – original draft (equal). **Daniele Ceneda**: Data curation (equal); Investigation (equal). **Daniele Scirè**: Resources (equal). **Mauro Mosca**: Resources (equal). **Dominique Persano Adorno**: Resources (equal). **Sina Abedini Dereshgi**: Data curation (equal); Formal analysis (equal). **Roberto Macaluso**: Investigation (equal); Resources (equal); Validation (equal); Writing – review & editing (equal). **Roberto Li Voti**: Data curation (equal); Formal analysis (equal); Methodology (equal); Validation (equal). **Concita Sibilia**: Conceptualization (equal); Formal analysis (equal); Investigation (equal); Validation (equal); Writing – review & editing (equal). **Tiziana Cesca**: Validation (equal). **Giovanni Mattei**: Validation (equal); Visualization (equal). **Koray Aydin**: Conceptualization (equal); Investigation (equal); Supervision (equal); Writing – review & editing (equal). **Marco Centini**: Conceptualization (equal); Data curation (equal); Formal analysis (equal); Investigation (equal); Methodology (equal); Supervision (equal); Writing – review & editing (equal).

DATA AVAILABILITY

The data that support the findings of this study are available from the corresponding author upon reasonable request.

REFERENCES

[1]H. Kocer, S. Butun, B. Banar, K. Wang, S. Tongay, J. Wu, and K. Aydin, "Thermal tuning of infrared resonant absorbers based on hybrid gold-VO$_2$ nanostructures," Appl. Phys. Lett. **106**, 161104 (2015).

[2]Y. Yao, R. Shankar, M. A. Kats, Y. Song, J. Kong, M. Loncar, and F. Capasso, "Electrically tunable metasurface perfect absorbers for ultrathin mid-infrared optical modulators," Nano Lett. **14**(11), 6526–6532 (2014).

[3]M. A. Butt, S. N. Khonina, N. L. Kazanskiy, and R. Piramidowicz, "Hybrid metasurface perfect absorbers for temperature and biosensing applications," Opt. Mater. **123**, 111906 (2022).

[4]W. W. Salisbury, "Absorbent body for electromagnetic waves," U.S. patent 2,599,944 (10 June 1952).

[5]M. C. Larciprete, M. Centini, R. Li Voti, and C. Sibilia, "Selective and tunable thermal emission in metamaterials composed of oriented polar inclusions," J. Opt. Soc. Am. B **34**(7), 1459–1464 (2017).

[6]R. Alaee, Y. Vaddi, and R. W. Boyd, "Dynamic coherent perfect absorption in nonlinear metasurfaces," Opt. Lett. **45**, 6414–6417 (2020).

[7]H. Kocer, S. Butun, E. Palacios *et al.*, "Intensity tunable infrared broadband absorbers based on VO$_2$ phase transition using planar layered thin films," Sci. Rep. **5**, 13384 (2015).

[8]M. A. Kats, D. Sharma, J. Lin, P. Genevet, R. Blanchard, Z. Yang, M. M. Qazilbash, D. Basov, S. Ramanathan, and F. Capasso, "Ultra-thin perfect absorber employing a tunable phase change material," Appl. Phys. Lett. **101**, 221101 (2012).

[9]S. Thongrattanasiri, F. H. L. Koppens, and F. J. García de Abajo, "Complete optical absorption in periodically patterned graphene," Phys. Rev. Lett. **108**, 047401 (2012).

[10]J. Rensberg, Y. Zhou, S. Richter, C. Wan, S. Zhang, P. Schöppe, R. Schmidt-Grund, S. Ramanathan, F. Capasso, M. A. Kats, and C. Ronning, "Epsilon-near-zero substrate engineering for ultrathin-film perfect absorbers," Phys. Rev. Appl. **8**, 014009 (2017).

[11]K. Halterman and J. Merle Elson, "Near-perfect absorption in epsilon-near-zero structures with hyperbolic dispersion," Opt. Express **22**, 7337–7348 (2014).

[12]A. Safaei, S. Chandra, M. N. Leuenberger and D. Chanda, "Wide angle dynamically tunable enhanced infrared absorption on large-area nanopatterned graphene," ACS Nano **13**(1), 421–428 (2019).

[13]D. Shrekenhamer, W.-C. Chen, and W. J. Padilla, "Liquid crystal tunable metamaterial absorber," Phys. Rev. Lett. **110**, 177403 (2013).

[14]S. Kim *et al.*, "Electronically tunable perfect absorption in graphene," Nano Lett. **18**, 971–979 (2018).

[15]M. C. Larciprete, M. Centini, S. Paoloni, I. Fratoddi, S. A. Dereshgi, K. Tang, J. Wu, and K. Aydin, "Adaptive tuning of infrared emission using VO$_2$ thin films," Sci. Rep. **10**, 11544 (2020).

[16]S. Abedini Dereshgi, M. C. Larciprete, M. Centini, A. A. Murthy, K. Tang, J. Wu, V. P. Dravid, and K. Aydin, "Tuning of optical phonons in α-MoO$_3$-VO$_2$ multilayers," ACS Appl. Mater. Interfaces **13**(41), 48981–48987 (2021).

[17]T. G. Sánchez, S. Amador-Alvarado, Y. Kumar, D. Ariza-Flores, M. A. Basurto-Pensado, and V. Agarwal, "Tailoring the UV–visible reflectivity range of VO$_2$ thin films," Mater. Lett. **323**, 132541 (2022).

[18]H. Kim, K. Cheung, R. C. Y. Auyeung *et al.*, "VO$_2$-based switchable radiator for spacecraft thermal control," Sci. Rep. **9**, 11329 (2019).

[19]H. Kim, D. Lahneman, C. Rohde, and A. Piqué, "VO$_2$-based thin-film radiators with variable thermal emissivity," Thin Solid Films **759**, 139455 (2022).

[20]J. Ge, Y. Zhang, H. Dong, and L. Zhang, "Nanolayered VO$_2$-based switchable terahertz metasurfaces as near-perfect absorbers and antireflection coatings," ACS Appl. Nano Mater. **5**(4), 5569–5577 (2022).

[21]A. Kaushal, N. Choudhary, N. Kaur, and D. Kaur, "VO$_2$–WO$_3$ nanocomposite thin films synthesized by pulsed laser deposition technique," Appl. Surf. Sci. **257**(21), 8937–8944 (2011).

[22]R. Macaluso, M. Mosca, V. Costanza, A. D'Angelo, G. Lullo, F. Caruso, C. Calì, F. Di Franco, M. Santamaria, and F. Di Quarto, "Resistive switching behaviour in ZnO and VO$_2$ memristors grown by pulsed laser deposition," Electron. Lett. **50**(4), 262–263 (2014).

[23]T. Cesca, C. Scian, E. Petronijevic, G. Leahu, R. Li Voti, G. Cesarini, R. Macaluso, M. Mosca, C. Sibilia, and G. Mattei, "Correlation between *in situ* structural and optical characterization of the semiconductor-to-metal phase transition of VO$_2$ thin films on sapphire," Nanoscale **12**, 851 (2020).

[24]V. V. Atuchin, T. Gavrilova, T. I. Grigorieva, N. Kuratieva, K. Okotrub, N. V. Pervukhina, and N. V. Surovtsev, "Sublimation growth and vibrational microspectrometry of α-MoO$_3$ single crystals," J. Cryst. Growth **318**, 987–990 (2011).

[25]M. Mosca, R. Macaluso, C. Calì, R. Butté, S. Nicolay, E. Feltin, D. Martin, and N. Grandjean, "Optical, structural, and morphological characterisation of epitaxial ZnO films grown by pulsed-laser deposition," Thin Solid Films **539**, 55 (2013).

[26]A. Boughelout, R. Macaluso, I. Crupi, B. Megna, A. Brighet, M. Trari, and M. Kechouane, "Effect of the Si doping on the properties of AZO/SiC/Si heterojunctions grown by low temperature pulsed laser deposition," Semicond. Sci. Technol. **36**, 015001 (2021).

[27]D. Scirè, R. Macaluso, M. Mosca, M. P. Casaletto, O. Isabella, M. Zeman, and I. Crupi, "Density of states characterization of TiO$_2$ films deposited by pulsed laser deposition for heterojunction solar cells," Nano Res. **15**, 4048–4057 (2022).

[28]A. Sacco, M. S. Di Bella, M. Gerosa, A. Chiodoni, S. Bianco, M. Mosca, R. Macaluso, C. Calì, and C. F. Pirri, "Enhancement of photoconversion efficiency in dye-sensitized solar cells exploiting pulsed laser deposited niobium pentoxide blocking layers," Thin Solid Films **574**, 38–42 (2015).

[29]M. C. Larciprete, M. Centini, S. Paoloni, S. A. Dereshgi, K. Tang, J. Wu, and K. Aydin, "Effect of heating/cooling dynamics in the hysteresis loop and tunable IR emissivity of VO$_2$ thin films," Opt. Express **28**, 39203 (2020).

[30]R. Li Voti, M. C. Larciprete, G. Leahu, C. Sibilia, and M. Bertolotti, "Optimization of thermochromic VO$_2$ based structures with tunable thermal emissivity," J. Appl. Phys. **112**, 034305 (2012).

[31]G. Cesarini, G. Leahu, A. Belardini, M. Centini, R. Li Voti, and C. Sibilia, "Quantitative evaluation of emission properties and thermal hysteresis in the mid-infrared for a single thin film of vanadium dioxide on a silicon substrate," Int. J. Therm. Sci. **146**, 106061 (2019).

[32]N. Zamani, A. Hatef, H. Nadgaran, and A. Keshavarz, "Control of electromagnetically induced transparency via a hybrid semiconductor quantum dot-vanadium dioxide nanoparticle system," J. Nanophotonics **11**(3), 036011 (2017).

[33]J. Rozen, R. Lopez, R. F. Haglund, Jr., and L. C. Feldman, "Two-dimensional current percolation in nanocrystalline vanadiumdioxide films," Appl. Phys. Lett. **88**, 081902 (2006).

[34]M. M. Qazilbash, M. Brehm, G. O. Andreev, A. Frenzel, P.-C. Ho, B.-G. Chae, B.-J. Kim, S. J. Yun, H.-T. Kim, A. V. Balatsky, O. G. Shpyrko, M. B. Maple, F. Keilmann, and D. N. Basov, "Infrared spectroscopy and nano-imaging of the insulator-to-metal transition in vanadium dioxide," Phys. Rev. B **79**, 075107 (2009).

[35]J. A. Ramirez-Rincon, C. L. Gomez–Heredia, A. Corvisier, J. Ordonez-Miranda, T. Girardeau, F. Paumier, C. Champeaux, F. Dumas-Bouchiat, Y. Ezzahri, K. Joulain, O. Ares, and J. J. Alvarado-Gil, "Thermal hysteresis measurement of the VO$_2$ dielectric function for its metal-insulator transition by visible-IR ellipsometry," J. Appl. Phys. **124**, 195102 (2018).

[36]A. A. Amooey, "Improved mixing rules for description of the permittivity of mixtures," J. Mol. Liq. **180**, 31–33 (2013).

[37]C. Wan, Z. Zhang, D. Woolf, C. M. Hessel, J. Rensberg, J. M. Hensley, Y. Xiao, A. Shahsafi, J. Salman, S. Richter, Y. Sun, M. M. Qazilbash, R. Schmidt-Grund, C. Ronning, S. Ramanathan, and M. A. Kats, "On the optical properties of thin-film vanadium dioxide from the visible to the far infrared," Ann. Phys. **531**, 1900188 (2019).

[38]J. Lekner, *Theory of Reflection* (Martinus Nijhoff Pubblisher, 1987).

[39]G. D'Aguanno, M. C. Larciprete, N. Mattiucci, A. Belardini, M. J. Bloemer, E. Fazio, O. Buganov, M. Centini, and C. Sibilia, "Experimental study of Bloch

12 September 2023 06:48:22

vector analysis in nonlinear, finite, dissipative systems," Phys. Rev. A **81**, 013834 (2010).

[40] D. G. Baranov, J. H. Edgar, T. Hoffman, N. Bassim, and J. D. Caldwell, "Perfect interferenceless absorption at infrared frequencies by a van der Waals crystal," Phys. Rev. B **92**, 201405 (2015).

[41] G. Hu, Q. Ou, G. Si, Y. Wu, J. Wu, Z. Dai, A. Krasnok, Y. Mazor, Q. Zhang, Q. Bao, C.-W. Qiu, and A. Alù, "Topological polaritons and photonic magic angles in twisted α-MoO₃ bilayers," Nature **582**, 209–213 (2020).

[42] G. Hu, W. Ma, D. Hu, J. Wu, C. Zheng, K. Liu, X. Zhang, X. Ni, J. Chen, X. Zhang, Q. Dai, J. D. Caldwell, A. Paarmann, A. Alù, P. Li, and C.-W. Qiu, "Real-space nanoimaging of hyperbolic shear polaritons in a monoclinic crystal," Nat. Nanotechnol. **18**, 64–70 (2023).

[43] H. Asayesh-Ardakani, W. Yao, A. Nie, P. M. Marley, E. Braham, R. F. Klie, S. Banerjee, and R. Shahbazian-Yassar, "Direct evidence of M₂ phase during the monoclinic-tetragonal (rutile) phase transition of W-doped VO₂ nanowires," Appl. Phys. Lett. **110**, 053107 (2017).

12 September 2023 06:48:22